Neuroradiology (1987) 29: 19-29

Neuroradiology

MR imaging in infra-, para- and retrosellar mass lesions

K. Sartor, M. G. Karnaze, J. D. Winthrop, M. Gado, F. J. Hodges, III.

Mallinckrodt Institute of Radiology, Section of Neuroradiology, Washington University School of Medicine, St. Louis, Missouri, USA

Summary. To determine its diagnostic efficacy in infra-, para- and retrosellar mass lesions magnetic resonance (MR) imaging was compared with computed tomography (CT) in 39 cases. Thirty-six lesions were imaged with a Siemens 0.5 T superconducting unit, three with a 1.5 T unit. CT scanning was performed with third generation equipment. There were 28 neoplasms including eight pituitary adenomas with infrasellar extension, four meningiomas, four extensions from regional malignancies, three chordomas, three juvenile angiofibromas, three medial temporal gliomas, and one each of neuroma, epidermoid and metastasis. Eleven non-neoplastic masses included four vascular anomalies, three cholesterol granulomas, two arachnoid cysts, one sphenoid mucocele and one mixed sclerosing bone dystrophy with mass-like thickening of basisphenoid and basiocciput. While MR and CT were equally sensitive (100%), MR was superior in further delineating and characterizing a lesion. MR showed normal or abnormal blood vessels better than CT, and revealed changes of compact bone often quite satisfactorily. Effects on the brain parenchyma or CSF and airspaces were consistently well demonstrated. Provided absence of contraindications MR should be the primary radiologic screening test in suspected mass lesions of above location.

Key words: Base of skull, magnetic resonance studies - Pituitary, neoplasms - Meninges, neoplasms - Paranasal sinuses and nasopharynx, abnormalities - Vascular anomalies

Space-occupying lesions that involve the sphenoid body, the basilar portion of the occipital bone, or their immediate vicinity, though pathologically quite diverse, may cause similar symptoms and signs. For the most part cranial nerve findings dominate the clinical picture, but depending on the location of the bulk of the mass partial complex seizures and long tract signs may also be observed. High resolution computed tomography (CT) has clearly become the mainstay in the diagnosis of such lesions [1-4], but is not without deficiencies. Angiography may still be needed to evaluate blood vessels or assess tumor vascularity [1, 4]. Bone artifacts are occasionally bothersome in the medial-most portion of the middle cranial fossa and around the clivus. Satisfactory direct coronal, let alone direct sagittal CT scanning [5], may not be feasible when desired. Moreover, CT is relatively unspecific. Recently, magnetic resonance (MR) imaging has been employed to examine the skull base with adjoining soft tissues [6-8]. This stimulated us to undertake a retrospective evaluation of our own case material with emphasis on a comparison between MR and CT. Our goal was to determine the diagnostic efficacy of the new imaging modality in above described lesions, i.e., infra-, para- and retrosellar/retroclival masses.

Material and methods

Reviewing the first 2000 neuroradiologic MR studies at our institution (August 1983-September 1985) we found 39 pertinent lesions. There were 28 neoplasms: eight mostly invasive pituitary adenomas with infrasellar and/or parasellar-parasphenoid extension, four meningiomas, four local extensions from regional malignancies, three chordomas, three juvenile angiofibromas, three medial temporal gliomas, and one each of plexiform neuroma, epidermoid, and metastasis. Pituitary adenomas with purely intrasellar or intra/suprasellar extension, brain-

Table 1. Summary of results

Lesion (#)	Morphologic Changes					Abnormal Signal	MR vs. CT		
	Brain	Blood Vessels	Bone	CSF-Spaces	Air-Spaces		Inferior	Equival.	Superior
Pituitary adenoma (8)	5	5	8	5	7	8	–	5	3
Meningioma (4)	4	4	3	4	1	4	–	4	–
Regional malignancy (4)	3	2	3	3	4	4	–	2	2
Chordoma (3)	3	3	3	3	3	3	–	–	3
Angiofibroma (3)	1	1	2	1	3	3	1	2	–
Glioma (3)	3	2	–	3	–	3	–	2	1
Metastasis (1)	1	–	–	1	–	1	–	1	–
Plexiform neuroma (1)	1	1	1	1	1	1	–	1	–
Epidermoid (1)	1	1	1	1	–	1	–	–	1
Vascular anomaly (4)	2	4	1	4	1	1[a]	1	1	2
Cholesterol granuloma (3)	–	–	3	1	3	3	–	1	2
Arachnoid cyst (2)	2	–	1	2	–	–	–	2	–
Bone dystrophy (1)	1	1	1	1	1	1	–	–	1
Sphenoid mucocele (1)	1	1	1	1	1	1	–	–	1

[a] Slightly increased signal intensity of brain parenchyma adjacent to AVM

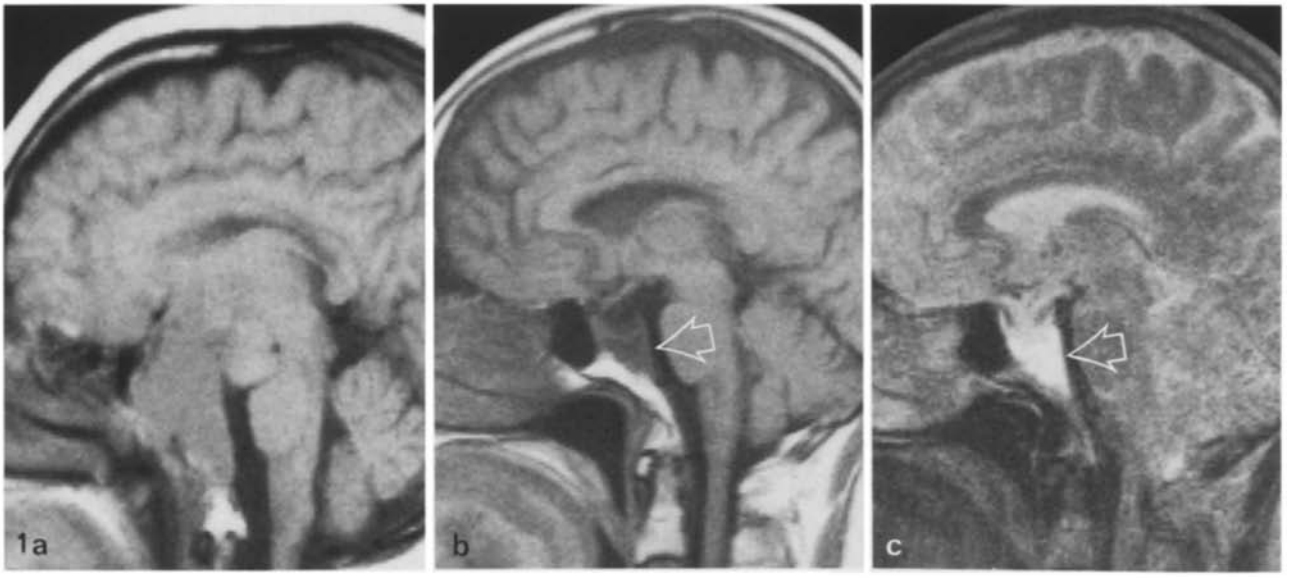

Fig. 1a–c. Invasive pituitary adenomas. (**a**) Sagittal SE 30/300 image shows infiltration of entire cancellous portion of clivus by prolactin-secreting adenoma with additional massive suprasellar extension. (**b**) Sagittal 30/300 image in another patient demonstrates partial infiltration of clivus by residual hormone-inactive adenoma. Note excellent contrast between neoplastic tissue *(arrow)* and normal bone marrow below. (**c**) Corresponding SE 120/1500 image reveals high signal of lesion reflecting long T2

stem gliomas, and acoustic neuromas were not included because their MR phenomenology has been amply described in the literature [7, 9–13, 17]. Other intrinsic brainstem lesions were also excluded for reasons of consistency. In addition to the 28 neoplasms, there were 11 non-neoplastic masses: four vascular anomalies, three cholesterol granulomas at the petrous apex, two arachnoid cysts, and one each of sphenoid mucocele, and mixed sclerosing bone dystrophy with marked thickening of basisphenoid and basiocciput. A tissue diagnosis was available in 21 of the 28 neoplastic lesions. Two pituitary adenomas, one chordoma, one glioma, the plexiform neuroma (in a patient with neurofibromatosis), the epidermoid (in a patient with a history longer than 10 years), and the metastasis (in a patient with malignant melanoma) were not pathologically proved. Surgical verification was also obtained in three of the non-neoplastic lesions, namely the mucocele and one each of the cholesterol granulomas and arachnoid cysts. All four vascular anomalies, two aneurysms, one arteriovenous malformation (AVM), and

one carotid-cavernous fistula, were confirmed by angiography.

MR imaging of 36 patients was performed with a 0.5 T superconducting Siemens imager (Erlangen, W. Germany) initially operated at 0.35 T. The remaining three patients were examined with a 1.5 T Siemens unit. A spin echo (SE) protocol was followed to obtain three images of the same anatomic level: T1-weighted (TR 300 or 500, TE 30 or 35 msec), spin density weighted (TR 1500 or 1800, TE 30 or 35 msec) and T2-weighted (TR 1500 or 1800, TE 120 msec). Multiple slice (interdigitated) images were obtained in various combinations of section planes, the most frequent one being coronal/sagittal. Coronal images were obtained in 80% of cases, sagittal images in 60% and axial in 10%. The slice thickness was 10 mm, except for one single study (5 mm). Images were reconstructed on a 256×256 matrix, corresponding to 1.0 mm^2 pixel size. Axial CT scanning - with intravenous contrast enhancement - was performed with third generation equipment (Siemens Somatom 2, DR 3, or DR H) with 2 or 4 mm contiguous sections. Coronal and sagittal reformations were generated in all cases. Direct coronal scans were obtained in five cases. All MR and CT studies were based on clinical indications.

MR images were scrutinized and any morphologic or signal abnormalities were recorded, each for the parenchymal, vascular, osseous, CSF- and air-compartments separately. The first three authors compared these changes with those shown on CT. MR was rated then *equivalent, superior,* or *inferior* by consensus based on subjective impression.

Results

A summary of results is presented in Table 1. No lesion demonstrated by CT was missed by MR. On the other hand, a small lesion of the petrous apex presumed to be a cholesterol granuloma was missed on the initial, standard CT scan (8 mm slice thickness). After its detection by MR the lesion was clearly demonstrated with high resolution CT and in retrospect could also be identified on the original scan. MR was rated *equivalent* to CT in 21 cases (54%), *superior* in 16 cases (41%), and *inferior* in 2 cases (5%). Superiority of MR over CT found its expression most frequently in an overall better demonstration of the extent of a given lesion including effects on neighboring structures, such as the cavernous sinus, the carotid, vertebral and basilar arteries, the medial temporal lobe, and the brainstem. Neoplastic invasion of the cancellous portion of the clivus, if present, was particularly well demonstrated on MR. In both cases where MR was thought to provide insufficient information volume averaging phenomena compounded by a somewhat sub-optimal image quality were the main reason.

Pituitary Adenomas

Three of eight tumors were diagnosed in the course of a work-up of patients with visual disturbances. The remainder represented residual (three) or recurrent (two) adenomas. Bony changes ranging from marked bulging of the eroded sellar floor into the sphenoid sinus to clear-cut invasion of the cancellous portion of the clivus were noted in all cases (Table 1). The latter phenomenon was observed in four of eight cases. On T1-weighted images bone invasion was characterized by low signal replacing the high signal of bone marrow (Fig. 1). With increasing T2-weighting the tumor signal exceeded that of the bone marrow. All adenomas were nearly isointense with brain (subcortical white matter) on the T1-weighted images and hyperintense on the spin density weighted and T2-weighted images. The highest signal (higher than CSF) was found in a residual mass encasing, but not compromising the cavernous portion of the carotid artery. Seven of the adenomas encroached upon the sphenoid sinus, and five distorted or displaced adjacent blood vessels, CSF-spaces and brain structures (Table 1). MR was equivalent to CT in five cases and superior in three. Superiority existed mainly with respect to the features of bone invasion, although effects on the cavernous sinus and the carotid arteries, e.g., displacement, invasion, encasement, were also very well shown.

Meningiomas

Three of the four tumors were residual lesions. Focally sclerotic or erosive bone changes were recognized in two of them as well as in a large foramen magnum meningioma diagnosed for the first time (Table 1). A prominent calcification in a residual parasellar meningioma was clearly identified as such, though less readily than with CT. All four meningiomas displaced, distorted or encased major arteries at the skull base, and all had local compressive effects on CSF-spaces and neural structures, including Meckel's cave in one case (Fig. 2). All tumors were practically isointense with the brain on T1-weighted images, and all demonstrated a mild to moderate signal increase on spin density weighted, and particularly on T2-weighted images. Encroachment on the sphenoid sinus was seen once. Although

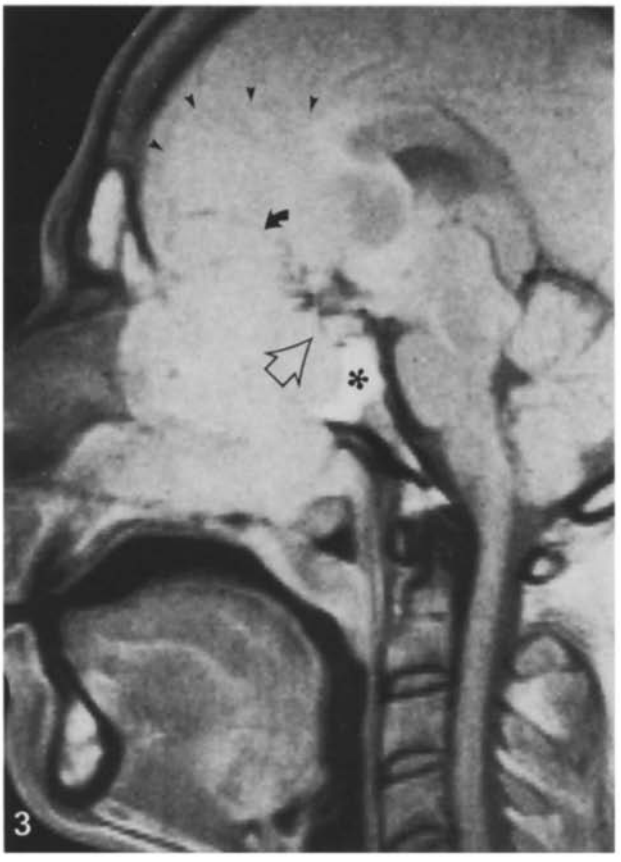

MR and CT were rated equivalent in all four meningiomas regarding diagnostic information provided, this information was more readily apparent on MR.

Regional Malignancy

Four malignant tumors, one lymphoma, one histiocytoma, one squamous cell, and one undifferentiated carcinoma, extended into the spheno-occipital region from the orbit or the upper airways. The mean feature of the squamous cell nasopharyngeal carcinoma was clival invasion, characterized by replacement of bone marrow by low signal tissue on T1-weighted images. All masses encroached on the sphenoid sinus and nasopharynx (Table 1). All lesions with intracranial extensions were isointense with the brain on short sequences and increased somewhat in signal intensity with more T2-weighting. Mild space occupying effects on CSF-spaces and brain were also noted in cases with intracranial extension. Displacement of major vessels was seen only twice (Table 1). In the two carcinomas the extent of the lesion was better evaluated with MR than with CT because of the higher contrast and the multiplanar visualization (Fig. 3).

Chordoma

All three lesions involved the clivus. Variable degrees of bone destruction along with space occupying effects on brainstem, blood vessels, cisterns, and air spaces were observed in all three cases (Table 1). On T1-weighted images these tumors were either isointense (2 cases) or hypointense (one case) compared to brain, but had all a conspicuously high signal intensity on T2-weighted images. On spin density weighted images they were isointense or slightly hyperintense. The relatively large posterior fossa component of one of the masses was not identified on CT due to bone induced artifacts (Fig. 4). In a second case axial and direct coronal CT scanning failed to demonstrate two tongue-like intracranial/intraspinal extensions clearly visible on MR (Fig. 5).

Fig. 2. Residual meningioma. Axial SE 30/300 image shows tumor invasion of Meckel's cave and cavernous sinus on left causing encasement of otherwise undisturbed carotid artery *(curved arrow)* as well as bulging of lateral sinus wall *(arrowheads)*. Asterisk marks posterior fossa component of tumor indenting pons and distorting basilar artery

Fig. 3. Undifferentiated carcinoma of nasal cavity. Sagittal SE 30/1500 image shows extensive destruction of medial frontal skull base including planum sphenoidale and anterior wall of sella (open arrow) with tumor extending far into intracranial space *(arrowheads)*. There is mucous retention in sphenoid *(asterisk)* as well as frontal sinuses, and superior bowing with tumor encasement of anterior cerebral arteries *(curved arrow)*

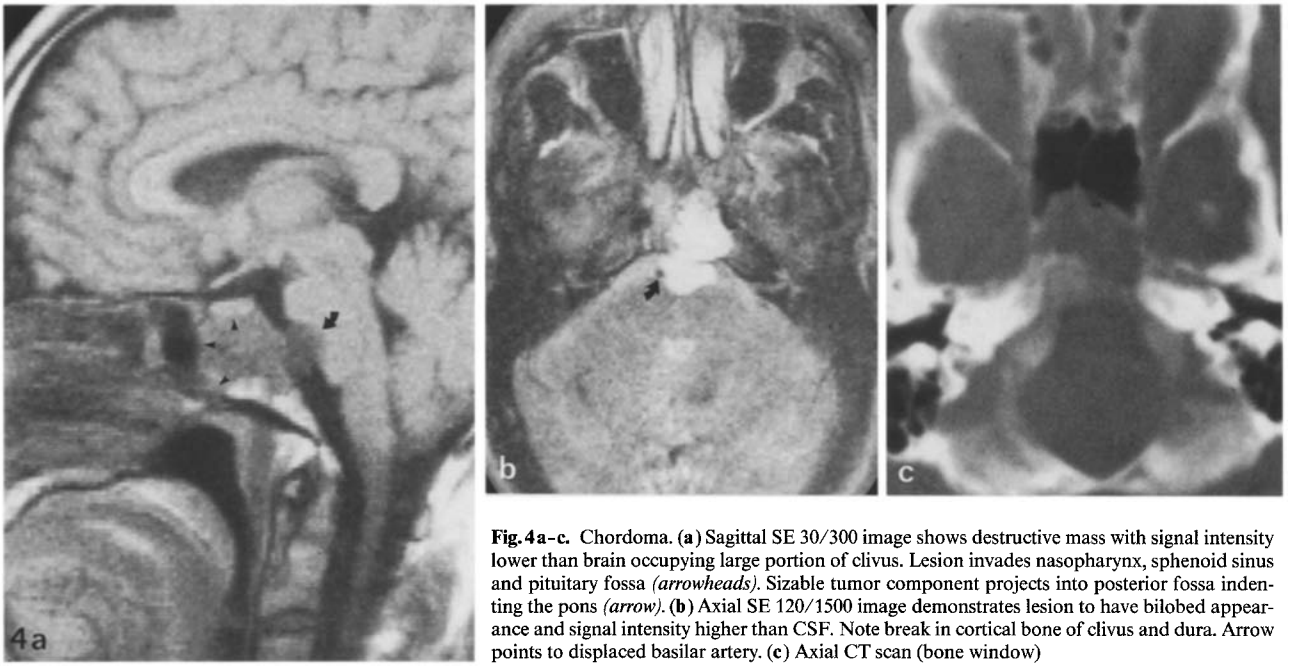

Fig. 4a–c. Chordoma. (**a**) Sagittal SE 30/300 image shows destructive mass with signal intensity lower than brain occupying large portion of clivus. Lesion invades nasopharynx, sphenoid sinus and pituitary fossa *(arrowheads)*. Sizable tumor component projects into posterior fossa indenting the pons *(arrow)*. (**b**) Axial SE 120/1500 image demonstrates lesion to have bilobed appearance and signal intensity higher than CSF. Note break in cortical bone of clivus and dura. Arrow points to displaced basilar artery. (**c**) Axial CT scan (bone window)

Angiofibroma

One of the three juvenile angiofibromas was a recurrent tumor. All three lesions were isointense with brain tissue on the T1-weighted and spin density weighted images, and had a significantly higher signal intensity on the T2-weighted scans. The highest signal was seen in the only mass with intracranial extension, however it was confined to the extracranial component. In fact, this portion had a multicystic appearance on MR as well as on CT. A follow-up MR study after embolization and radiation therapy revealed a marked reduction in size of the mass, with disappearance of the intracranial component and remodelling of the anterior and middle cranial fossae (Fig. 6). Osseous changes were present in all cases according to the CT scans but were detected only twice by MR. The soft tissue mass itself was consistently well outlined as it encroached upon the air within the sinuses and nasopharnyx (Table 1).

Glioma

All three tumors involved the medial portion of the temporal lobe and exhibited an abnormal signal: in two, a proved ganglioglioma and a presumed low grade glioma, both with calcifications, the lesion was isointense with normal brain on T1-weighted images, slightly hyperintense on spin density weighted images, and moderately or markedly hyperintense on T2-weighted images. While the large calficiation of the presumed low grade glioma was appreciated on MR as a signal-void area, the small calcification of the ganglioglioma was not. In the latter case, however, CT only demonstrated the calcification and provided no evidence of a tissue alteration; the decision to operate was significantly influenced by the MR result. In the third case, a proved astrocytoma grade II–III without calcification, the lesion was hypointense on T1-weighted images, and moderately hyperintense on spin density and T2-weighted images. Mild displacement of carotid and middle cerebral arteries was noted in two of the three cases, mass effects on CSF spaces in all of them (Table 1).

Miscellaneous Neoplastic Lesions

The single metastasis involved Meckel's cave and was characterized by a signal behavior different from CSF which normally fills much of this space. It was isointense with brain on T1 and T2-weighted images. The plexiform neuroma was an intracranial parasellar-parasphenoid extension of a huge hemifacial lesion that also involved the orbit. Meckel's cave appeared ectatic but otherwise undisturbed. Changes of the sphenoid bone, some of them dysplastic, others probably due to pressure erosion, were better discerned on CT, while the relationship between the medially displaced carotid artery and the mass was more easily appreciated on MR. The presumed epidermoid tumor and its effects on the carotid artery and the temporal lobe were more clearly depicted by MR than CT (Fig. 7).

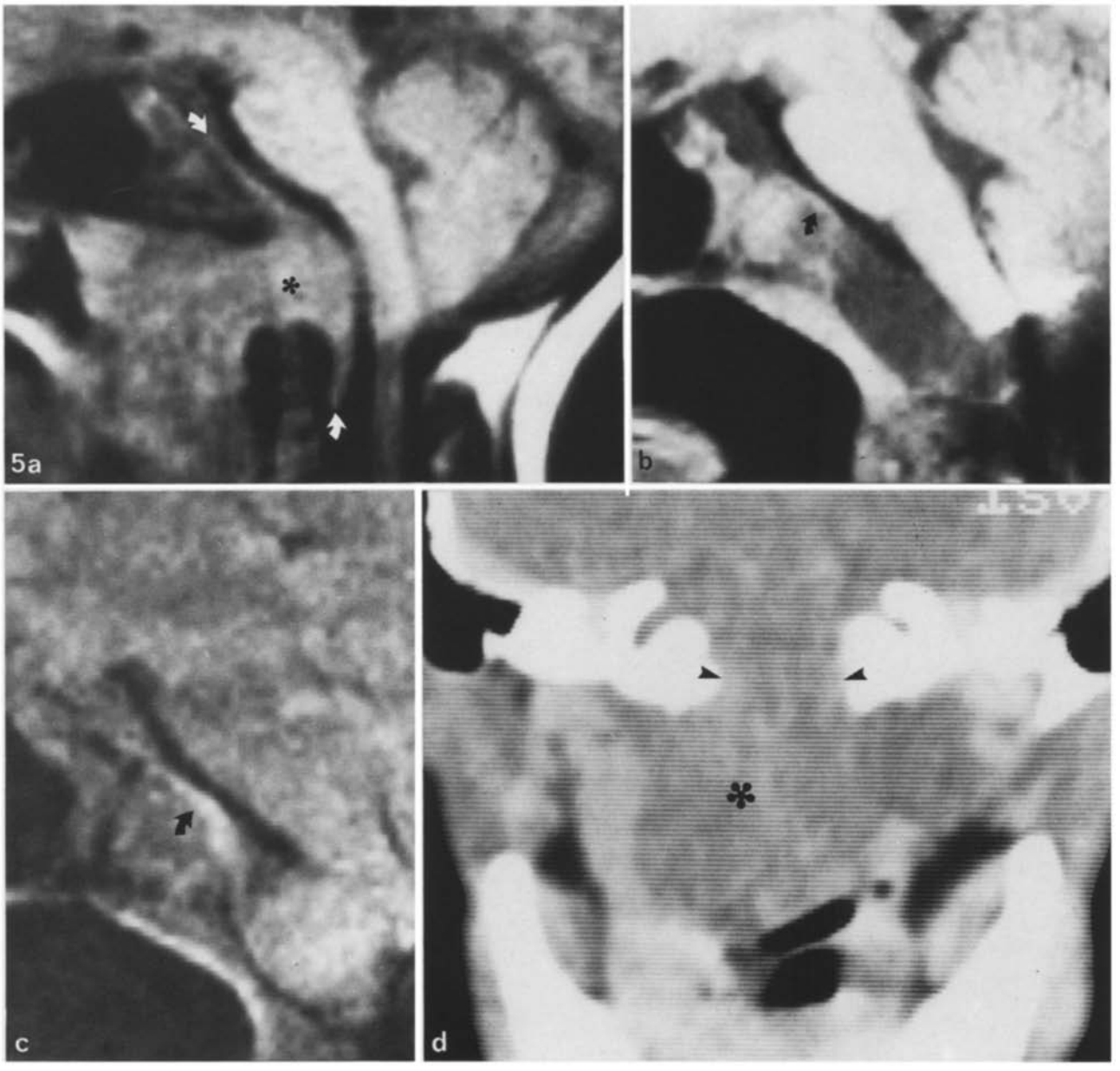

Fig. 5a–d. Chondroid chordoma in a child. (**a**) Sagittal SE 35/500 image shows bulk of mass within nasopharynx. Large component involves craniospinal junction (asterisk) eroding clivus as well as odontoid process and projecting into posterior fossa with tongue-like tumor extensions on back of clivus and behind odontoid *(arrows)*. Note distortion of lower brainstem. (**b**) Sagittal SE 35/500 image after subtotal resection. Curved arrow points to remaining tumor "tongue". Limited image distortion at craniospinal junction due to artifact from fairly large metallic implant for stabilization purposes. (**c**) Corresponding SE 120/1800 image demonstrates residual tissue *(arrow)* better. (**d**) Coronal contrast CT scan reveals only bulk of lesion *(asterisk)* and destruction of lower clivus *(arrowheads)*

Vascular Anomaly

One of the two aneurysms, arising from the basilar artery, was poorly demonstrated on sagittal MR images due to volume averaging and motion artifacts. The other aneurysm involved the cavernous portion of the carotid artery and could be better evaluated using MR. CT, though suggesting the vascular nature of the parasphenoid mass, was not unequivocal (Fig. 8). MR also allowed a more rapid and reliable distinction between tumor and vascular anomaly in the medial temporal AVM. The slight signal increase of some of the brain tissue surrounding the black appearing anomalous vessels (on spin density and T2-weighted images) was believed to be due to chronic ischemic changes. The carotid-cavernous fis-

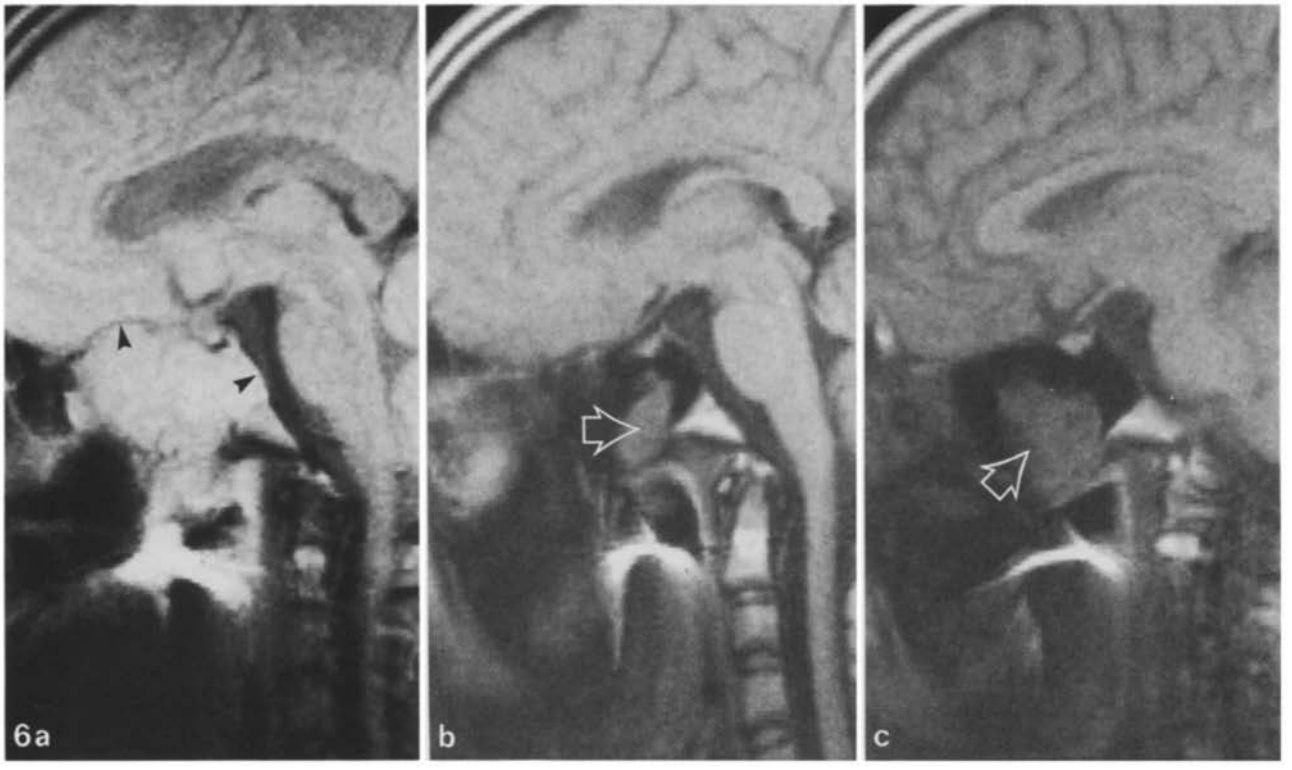

Fig. 6a–c. Juvenile angiofibroma. (**a**) Sagittal SE 30/1500 image shows tumor to involve, in addition to part of nasopharynx, posterior portion of ethmoid labyrinth and entire sphenoid sinus with encroachment on intracranial space in two locations *(arrows)*. (**b**) and (**c**) Sagittal/parasagittal SE 30/300 images about six months after embolization and full course of radiation reveal marked shrinkage of tumor *(arrows)* plus remodelling of formerly distorted and focally eroded sphenoid walls. Local artifact results from vascular clip

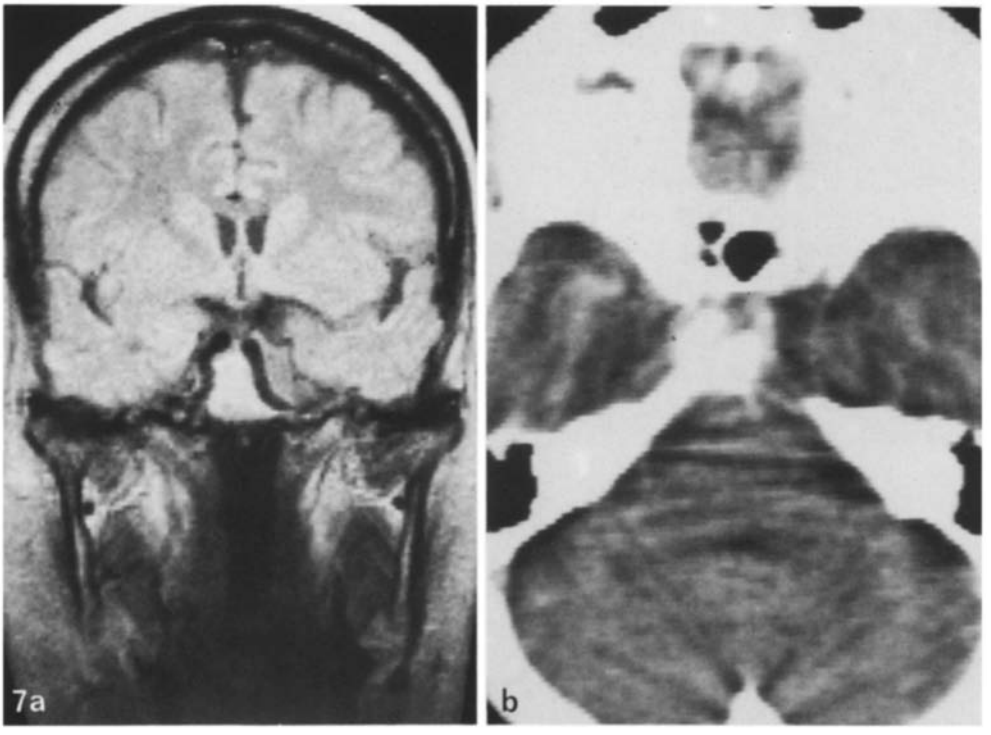

Fig. 7a and b. Presumed epidermoid. (**a**) Coronal SE 30/1500 image shows parasellar/parasphenoid mass on left; lesion is about isointense with subcortical white matter. Medially displaced but otherwise uncompromised carotid artery well contrasted against high signal from cancellous portion of basisphenoid. Note clear demarcation between mass and temporal lobe. (**b**) Axial contrast CT scan fails to demonstrate full extent of lesion and visualize carotid artery satisfactorily

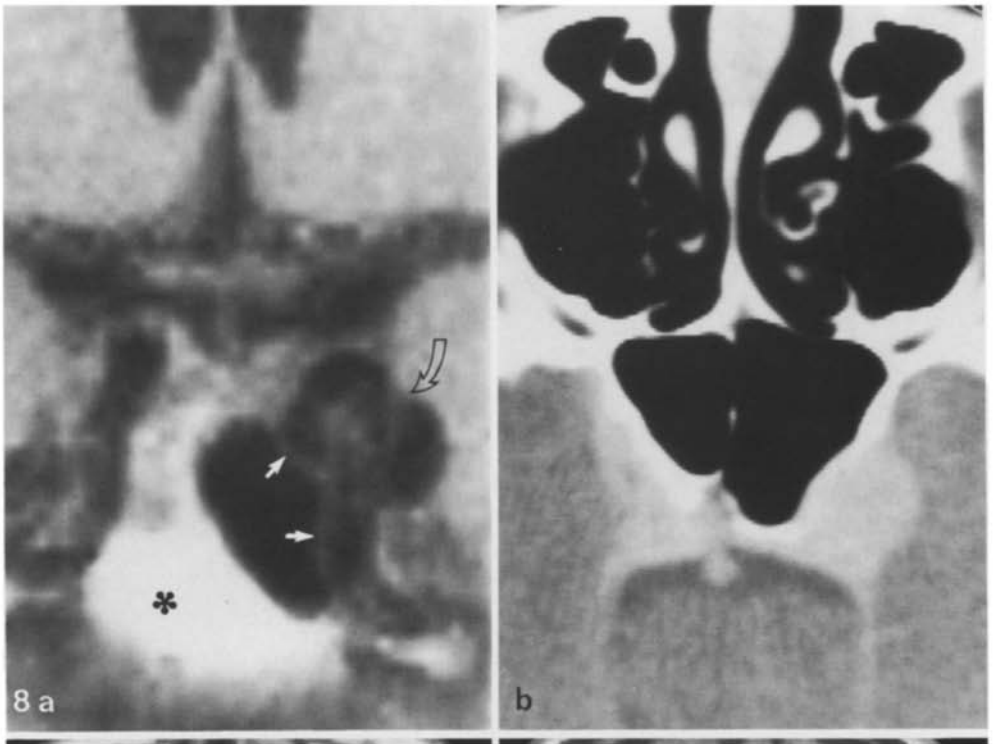

Fig. 8 a and b. Carotid aneurysm. (**a**) Coronal SE 30/300 image shows lesion *(curved arrow)* to arise from posterior cavernous portion of left internal carotid artery. High signal of center of lesion suggests partial thrombosis. Arrows superimposed on ipsilateral sphenoid sinus point to medial walls of aneurysm and carotid artery, respectively. Asterisk denotes cancellous portion of basisphenoid. (**b**) Axial contrast CT scan reveals enhancing parasellar mass but is non-specific

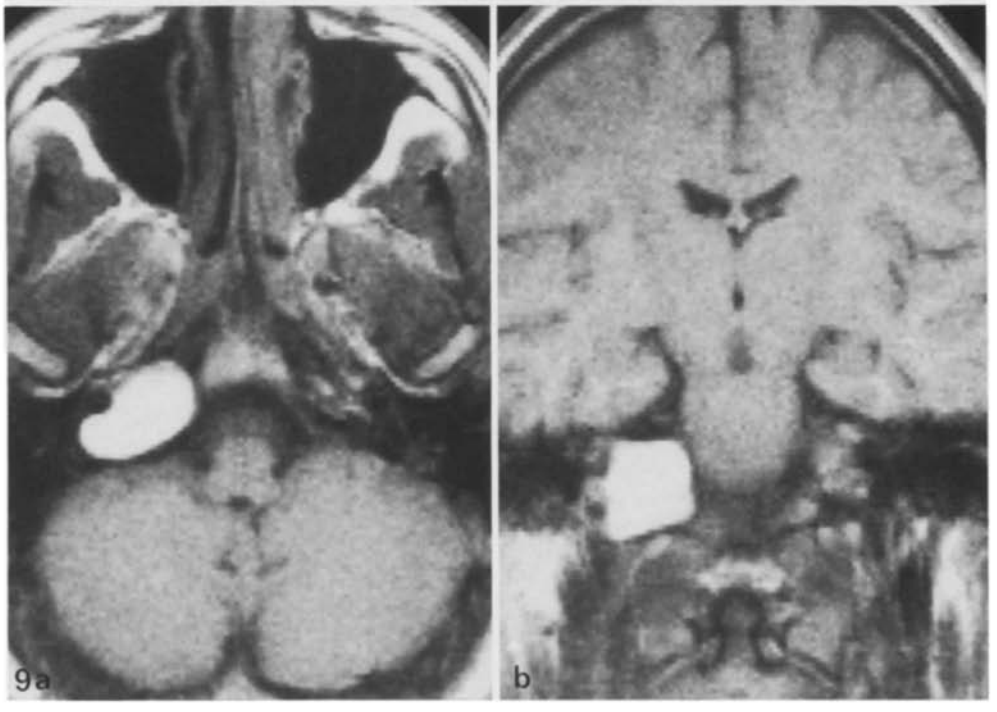

Fig. 9 a and b. Cholesterol granuloma. (**a**) Axial SE 30/300 image shows expansile high signal lesion originating from right petrous apex; mass abuts clivus medially. (**b**) Coronal SE 30/300 image

tula was equally well demonstrated with both imaging modalities.

Cholesterol Granuloma

The largest of the three lesions was operated on and pathologically proved; it was equally well shown by MR and CT (Fig. 9). The other two, both incidental findings, were significantly smaller and diagnosed on the basis of the criteria given by Lo et al. [14]. Owing to their very high signal intensity, especially on T1-weighted images, they were much more easily recognized on MR.

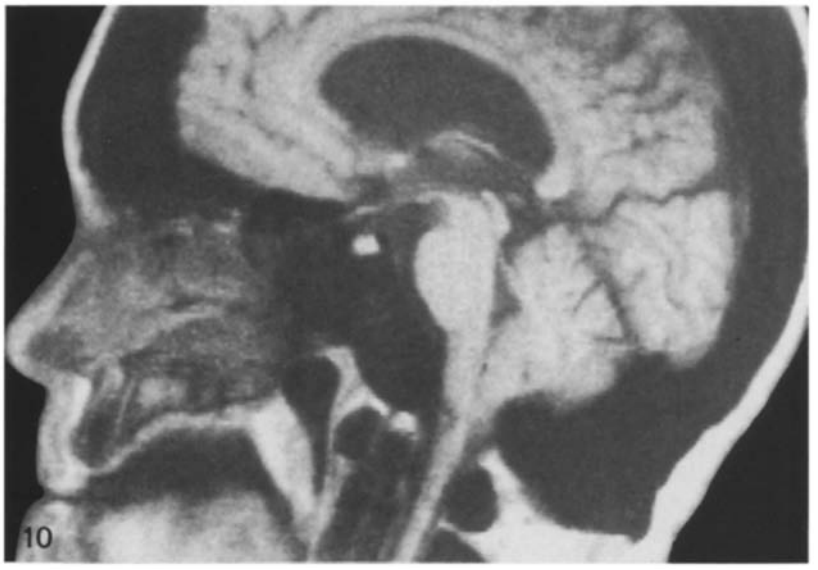

Fig. 10. Diffuse mixed sclerosing bone dystrophy. Sagittal SE 30/300 image shows generalized thickening and sclerosis of calvarium, skull base, and upper cervical spine, with basisphenoid and basiocciput having compact bone appearance; sphenoid sinus obliterated. Note encroachment of clivus on lower brainstem

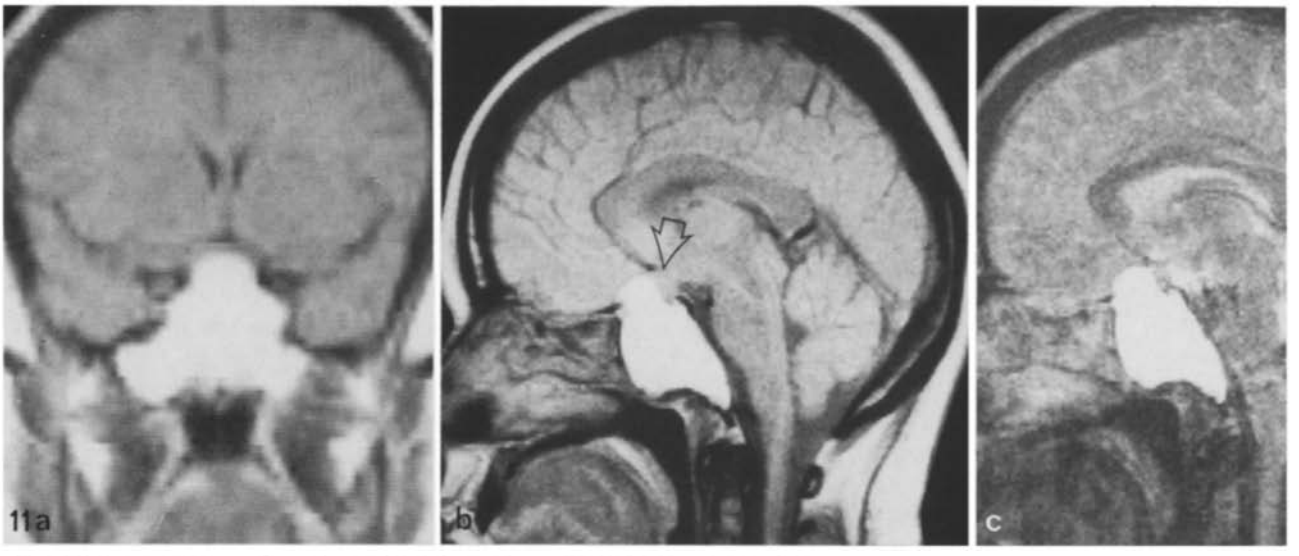

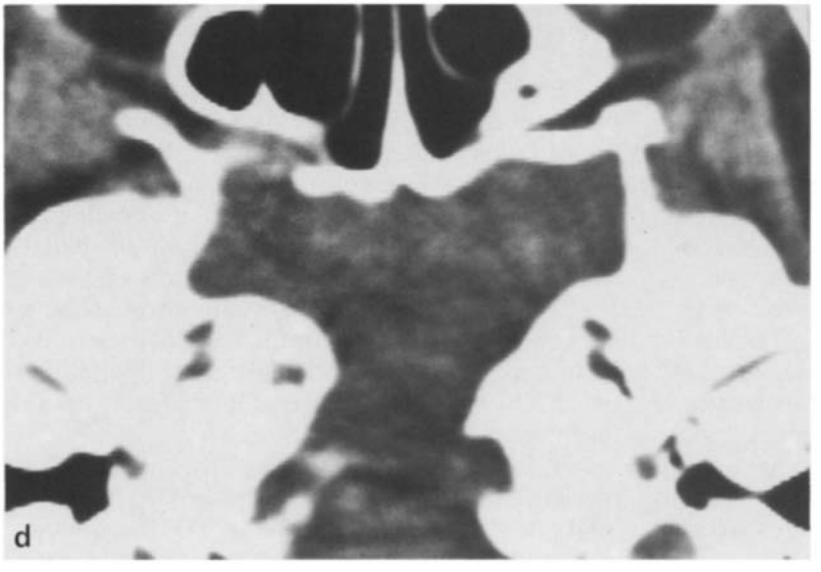

Fig. 11 a–d. Sphenoid mucocele. (**a**) Coronal SE 30/300 image shows markedly expanded sphenoid sinus homogeneously filled with high signal material (short T1). (**b**) Sagittal SE 30/1500 image reveals erosion of planum sphenoidale and sellar floor with suprasellar expansion of lesion. Arrow points to elevated, but otherwise normal, pituitary gland. Retained fluid has much higher signal than brain. (**c**) Corresponding SE 120/1500 image demonstrates still very high signal of fluid (long T2). (**d**) Axial contrast CT scan leaves doubt as to true nature of "mass"

Miscellaneous Non-Neoplastic Lesions

The two arachnoid cysts were rather small and behaved on MR essentially like locally widened CSF spaces. Focal bony changes were noted in one case (Table 1). In terms of diagnostic quality no marked difference between MR and CT was found, though MR was more convincing that the lesion was extraaxial in nature and did not represent, for example, a low grade glioma [15]. The bone dystrophy was of the diffuse mixed-sclerosing type and had led to a marked thickening of the clivus and other parts of the skull base reducing the space available for the lower portions of brainstem and cerebellum. In addition, the entire sphenoid sinus was obliterated by dense bone. These changes were best shown on the sagittal MR images (Fig. 10). The MR appearance of the sphenoid mucocele was specific, unlike its plain film and CT appearances, which did not entirely exclude the possibility of a less benign process. The homogeneous signal of the retained secretions, highest on the T2-weighted images, was hyperintense even on the T1-weighted scans suggesting a high fat content and/or previous hemorrhage. The effects of the lesion on intracranial structures including the carotid arteries and the pituitary gland was also better demonstrated by MR than CT (Fig. 11).

Discussion

The infra-, para- and retrosellar region is characterized by a wide range of pathology with certain similarities of clinical presentation. Although high resolution CT has proved very useful [1–4], there are disadvantages of this diagnostic modality, the most important ones being the difficulty of obtaining good quality direct scans in more than one plane *throughout* the area, the limited soft tissue visualization near bone, and the frequent need for administration of intravenous contrast media. According to our results MR is essentially free of these deficiencies. Its well known strengths, namely multiplanar capability, excellent contrast resolution with absence of bone induced artifacts, and spontaneous demonstration of blood vessels were advantageous in several ways: First, MR often provided improved lesion delineation in all three dimensions, including assessment of intraaxial, extraaxial, extradural, or combined extension, while maintaining a lesion detection rate equal to CT (100%). Since masses of the infra-, para- and retrosellar region involve a rather remote and anatomically complex part of the intracranial space, a very precise determination of their topography, extent, and character is necessary prior to treatment. In our series MR was clearly more helpful than CT in that respect in 41% of cases. Furthermore, major arteries including their morphologic changes, e. g., widening, narrowing and displacement, were consistently better shown by MR. This was especially true when marked contrast enhancement of a lesion obscured the vascular encroachment or encasement. On MR, as long as there is sufficient flow, the signal difference between the lesion and the (dark) vessel is striking (Fig. 2). By the same token MR helped to separate aneurysms or AVMs from tumors with high vascularity (Fig. 8). Although MR is regarded as generally inferior to CT with respect to visualizing bony structures (and calcifications), our data indicate that this is not always true when examining the skull base, including delicate compact bone such as the sellar floor (Figs. 3 and 11). Abnormalities of cancellous bone were even better demonstrated with MR than with CT, an observation also made by others [6]. Primarily because of this, the overall superiority of MR was most convincing in the invasive pituitary adenomas, chordomas, and regional malignancies that involved the clivus (Figs. 1 and 4). Even the limited specificity of MR is still higher than that of CT. Our results showed characterization and precise delineation of extent of lesions by MR to be superior to CT in 41% and equal in 54% of cases. This suggests that MR may be recommended as the more effective method of evaluation in the sphenooccipital region. Finally, the lack of radiation of MR may be regarded as an added bonus, perhaps most welcome in young patients who need to be followed closely or for a long period of time. The child with the chondroid chordoma in our series is being followed exclusively by MR, partly also because MR images, in contrast to CT scans, are relatively immune to the detrimental affects of larger metallic implants [16] (Fig. 5).

Diagnostic weaknesses of MR that became apparent in our analysis were primarily linked to the use of rather thick sections (10 mm). Thinner slices, similar to the ones employed in high resolution CT, result in less volume averaging and are clearly preferable, provided imaging time is not unduly lengthened. High field strength MR scanners (1.0 T and above) seem to be best suited for this purpose [17]. In a number of lesions, specifically some of the extraaxial tumors, intravenous administration of Gadolinium-DTPA may have been useful and improved the diagnostic quality of MR [18].

In conclusion, with respect to infra-, para- and retrosellar mass lesions and compared to CT, MR might be characterized as follows: (1) has equal detection power, (2) determines margins and topographic relationships in a superior fashion, (3) dem-

onstrates blood vessels and their changes more convincingly, in more detail, and without intravenous contrast enhancement, (4) possesses higher sensitivity for tumor invasion and other obliterative changes of cancellous bone, (5) shows changes involving compact bone to some extent, albeit not as consistently as CT, and (6) allows a more specific diagnosis than CT in a number of cases. Therefore, because MR is more likely to answer the relevant questions, it should be the primary radiologic screening test whenever such a lesion is suspected and none of the known contraindications exists. Likewise MR is better suited for follow-up, especially in children.

Acknowledgement. The authors would like to express their gratitude to Ms. Nancy North for the preparation of the manuscript, and to Mr. Norman Hente and Mr. Thomas Murray for the photographic work.

References

1. Bryan RN, Sessions RB, Horowitz BL (1981) Radiographic management of juvenile angiofibromas. AJNR 2: 157-166
2. Taylor S (1982) High resolution computed tomography of the sella. Radiol Clin North Am 10: 207-236
3. Kapila A, Chakeres DW, Blanco E (1984) The Meckel cave: Computed tomographic study. Radiology 152: 425-433
4. Moore T, Ganti SR, Mawad ME, Hilal SK (1985) CT and angiography of primary extradural juxtasellar tumors. AJNR 6: 521-526
5. Osborn AG, Anderson RE (1978) Direct sagittal computed tomography scans of the face and paranasal sinuses. Radiology 129: 81-87
6. Han JS, Huss RG, Benson JE, Kaufman B, Yoon YS, Morrison SC, Alfidi RJ, Rekate JL, Ratcheson RA (1984) MR imaging of the skull base. J Comput Assist Tomogr 8: 944-952
7. Lee BCP, Kneeland JB, Deck MDF, Cahill PT (1984) Posterior fossa lesions: Magnetic resonance imaging. Radiology 153: 137-143
8. Lee BCP, Deck MDF (1985) Sellar and juxtasellar lesion detection with MR. Radiology 157: 143-147
9. Randell CP, Collins AG, Young IR, Haywood R, Thomas DJ, McDonnell MJ, Orr JS, Bydder GM, Steiner RE (1983) Nuclear magnetic resonance imaging of posterior fossa tumors. AJNR 4: 1027-1034
10. Han JS, Bonstelle CT, Kaufman B, Benson JE, Alfidi RJ, Clampitt M, Van Dyke C, Huss RG (1984) Magnetic resonance imaging in the evaluation of the brainstem. Radiology 150: 705-712
11. Kingsley DPE, Brooks BG, Leung A W-L, Johnson MA (1985) Acoustic neuromas: Evaluation by magnetic resonance imaging. AJNR 6: 1-5
12. New PFJ, Bachow TB, Wisner GL, Rosen BR, Brady TJ (1985) MR imaging of the acoustic nerves and small acoustic neuromas at 0.6 T: Prospective study. AJNR 6: 165-170
13. Hueftle MG, Han JS, Kaufman B, Benson JE (1985) MR imaging of brain stem gliomas. J Comput Assist Tomogr 9: 263-267
14. Lo WWM, Solti-Bohman LG, Brackmann DE, Gruskin P (1984) Cholesterol granuloma of petrous apex: CT diagnosis. Radiology 153: 705-711
15. Aaron J, New PFJ, Strand R, Beaulieu P, Elmden K, Brady TJ (1984) NMR imaging in temporal lobe epilepsy due to gliomas. J Comput Assist Tomogr 8: 608-613
16. Laakman RW, Kaufman B, Han JS, Nelson AD, Clampitt M, O'Block AM, Haaga JR, Alfidi RJ (1985) MR imaging in patients with metallic implants. Radiology 157: 711-714
17. Bilaniuk LT, Zimmerman RA, Wehrli FW, Snyder PJ, Goldberg HI, Grossman RI, Bottomley PA, Edelstein WA, Glover GH, MacFall JR, Redington RW (1984) Magnetic resonance imaging of pituitary lesions using 1.0 to 1.5 T field strength. Radiology 153: 415-418
18. Felix R, Schörner W, Laniado M, Niendorf H-P, Claussen C, Fiegler W, Speck U (1985) Brain tumors: MR imaging with Gadolinium-DTPA. Radiology 156: 681-688

Received: 10 June 1986

Klaus Sartor, M. D.
Mallinckrodt Institute of Radiology
Washington University School of Medicine
510 South Kingshighway Blvd.,
St. Louis, Missouri 63110, USA